Computational metallurgy and changes of scale / Métallurgie numérique et changements d'échelle

Scale transitions in crystal plasticity by dislocation dynamics simulations

Transitions d'échelle en plasticité utilisant des simulations de dynamique des dislocations

Benoit Devincre *, Ladislas Kubin

Laboratoire d'étude des microstructures, CNRS-ONERA, 29, avenue de la Division Leclerc, BP 72, 92322 Châtillon cedex, France

ABSTRACT

This article shows, on the base of recent results, that dislocation dynamics simulations provide a unique opportunity for establishing scale transitions in crystal plasticity. In the present study, transitions are performed between elementary dislocation mechanisms, collective and intermittent slip events at the mesoscale and the mechanical response of bulk materials with low lattice resistance. In fcc crystals, the insight that is obtained provides guidelines for the modeling of collective dislocation behavior. It also allows incorporating more physical input into phenomenological models for strain hardening and improving their predictive ability.

© 2010 Académie des sciences. Published by Elsevier Masson SAS. All rights reserved.

RÉSUMÉ

Cet article basé sur des résultats récents illustre l'énorme potentiel que présentent les simulations de dynamique des dislocations pour effectuer des transitions d'échelle en plasticité. La présente étude concerne les transitions entre les propriétés élémentaires des dislocations, le comportement intermittent associé au glissement à l'échelle mésoscopique et la réponse mécanique des matériaux massifs à faible friction de réseau. Dans le cas des monocristaux cfc, la vision ainsi obtenue est mise à profit pour guider la modélisation du comportement collectif des dislocations. Elle permet également d'incorporer davantage de physique dans les modèles phénoménologiques pour le durcissement d'écrouissage et d'améliorer leur caractère prédictif.

© 2010 Académie des sciences. Published by Elsevier Masson SAS. All rights reserved.

1. Introduction

When forces are applied to a crystalline material, it may deform in an irreversible, or plastic, manner. This property is essential in two ways. First, it allows performing the shape transformations involved during the processing of engineering materials. Second, in service conditions, these materials can accommodate an overload by plastic deformation instead of breaking abruptly. The observation of slip traces at the surface of deformed specimens and, later on, the advent of dislocation theory, clearly showed that plasticity is a discrete and non-uniform process mediated by crystal defects. Nevertheless, material scientists are currently modeling "plastic flow" as a continuous and uniform process having some remote similitudes with viscous flow in liquids [1]. To date, dislocation theory can explain reasonably well the properties of individual dislocations [2,3], but is still unable to deal with their collective properties. This transition between discrete and uniform

---

* Corresponding author.
  E-mail address: benoit.devincre@onera.fr (B. Devincre).

plastic flow is one of the reasons why establishing a multiscale theory of plasticity having a predictive ability and based on dislocation properties remains a formidable challenge. In the past few years, the development of micro- and nanotechnologies made it even clearer that there is an urgent need for physically justified plasticity models.

The multiscale modeling of plasticity was initiated near the end of the last century [4]. In this bottom-up approach, electronic structure and atomistic simulations allow investigating dislocation core properties and yield insight into thermally activated processes like cross-slip or dislocation mobility in materials with high lattice resistance. These properties serve as input for simulations operating at the mesoscale, which is the scale of the dislocation microstructure. Ultimately, data from mesoscale simulations have to be incorporated into the continuum mechanical tools that are currently used to solve the behavior of engineering materials under complex loading conditions. The three-dimensional simulations of dislocation dynamics (DD) are now a critical part of the present effort at establishing such a multiscale modeling framewok [5,6]. They operate at the mesoscopic scale and their main fundamental objective is to establish bridges between the discrete, collective and continuous descriptions of crystal plasticity.

DD simulations compute plastic deformation by integrating the equations of motion of dislocation lines under stress in an elastic continuum. The mutual interactions of dislocations, the formation and destruction of junctions, their line tension and their interactions with other defects are drawn from the elastic theory of dislocations. In addition, local rules are implemented, which account for specific dislocation core properties.

Fig. 1 shows typical examples of stress–strain curves obtained by such DD simulations, which illustrate an important feature of plasticity. Applying periodic boundary conditions to a primary simulation cell allows monitoring a representative volume of macroscopic sample at the scale of a few tens of microns. Depending on the material considered, plastic flow is either smooth (Fig. 1a), or proceeds in a jerky manner (Figs. 1b and 1c). In what follows, the focus is on this serrated flow observed in DD simulations, which was recently shown to reflect the occurrence of a collective, scale-free and intermittent, dislocation behavior [7,8].

2. Dislocation glide

In many materials, a strong lattice resistance arises from either the non-metallic nature of bonding or the propensity of screw dislocations cores to adopt sessile (immobile), non-planar configurations of low energy. Then, the dislocations move by a specific thermally activated process, the kink-pair mechanism, which involves the generation and sideways expansion of kink pairs along the lines. As a consequence, the mechanical response reflects the resulting low intrinsic mobility. This is for instance the case in bcc metals like α-iron at low temperatures, in which a high lattice resistance arises from the three-dimensional spreading of the cores of $\frac{1}{2}\langle 111 \rangle$ screw dislocations.

As a rule, all dislocations submitted to a high lattice resistance move in a crystal with similar low velocities, because they are overcoming the same dense and strong obstacles to their motion, the atomic rows. Most of the screw dislocations must be mobile in order to yield the imposed plastic strain rate. This explains why the simulated stress–strain curves shown in Fig. 1a are smooth. The same type of smooth behavior is observed when adding a large density of carbide precipitates. Even if these precipitates usually behave as strong obstacles, they induce only a small strengthening τ_{obs} in iron at low temperature. The reason is that the screw lines are not blocked between obstacles and can still move by the kink-pair mechanism. Hence, in this example, the effective stress τ^* required to overcome the lattice resistance is still large compared to the obstacle strength ($\tau^* \gg \tau_{obs}$) and dislocation glide is continuous at the mesoscopic scale.

Alternatively, when the lattice resistance is low, the intrinsic dislocation mobility is high. The short- and long-range interactions between dislocations, which are athermal, govern plastic flow. The yield stress is then much smaller than in the previous case. Among the typical materials where the dislocation–dislocation interactions govern plastic flow, one finds fcc metals (Fig. 1c) and bcc metals above their athermal temperature, that is, the temperature above which the whole activation energy for the kink-pair mechanism is furnished by the lattice vibrations (Fig. 1b). Obstacle strengthening can be significant in these materials ($\tau_{obs} > \tau^*$) and the behavior of the mobile dislocations drastically differs from the one imposed by the kink-pair mechanism. Line tension effects govern the bowing out of the lines between obstacles and only a small fraction of the total dislocation density is mobile at a given moment. Between obstacles, the free-flight velocity of the dislocations is large and is controlled by their interactions with phonon modes. In conventional deformation conditions, this dissipation process is expressed by a linear relation between the steady-sate velocity υ and the effective stress:

$$\upsilon = \tau^* b / B(T) \tag{1}$$

where b is the modulus of the Burgers vector of the dislocations and $B(T)$ is a viscous drag coefficient, which depends on temperature via the properties of the phonon spectrum and saturates at the Debye temperature. The drag constant, which appears at the input of DD simulations, can be measured experimentally. It can also be estimated from atomistic simulations, but this requires some care [11].

In pure materials with low lattice resistance, the dislocation–dislocation interactions induce complex collective effects. To illustrate this property, DD simulations were performed using artificially increased values of the drag constant B in order to shift the balance between dislocation interactions and viscous drag. The results are shown in Fig. 2.

For the largest values of B, that is, for low intrinsic dislocation velocities, plastic flow is continuous with a flow stress proportional to the dislocation mobility. In such conditions where the free-flight velocity governs plastic flow, the increase
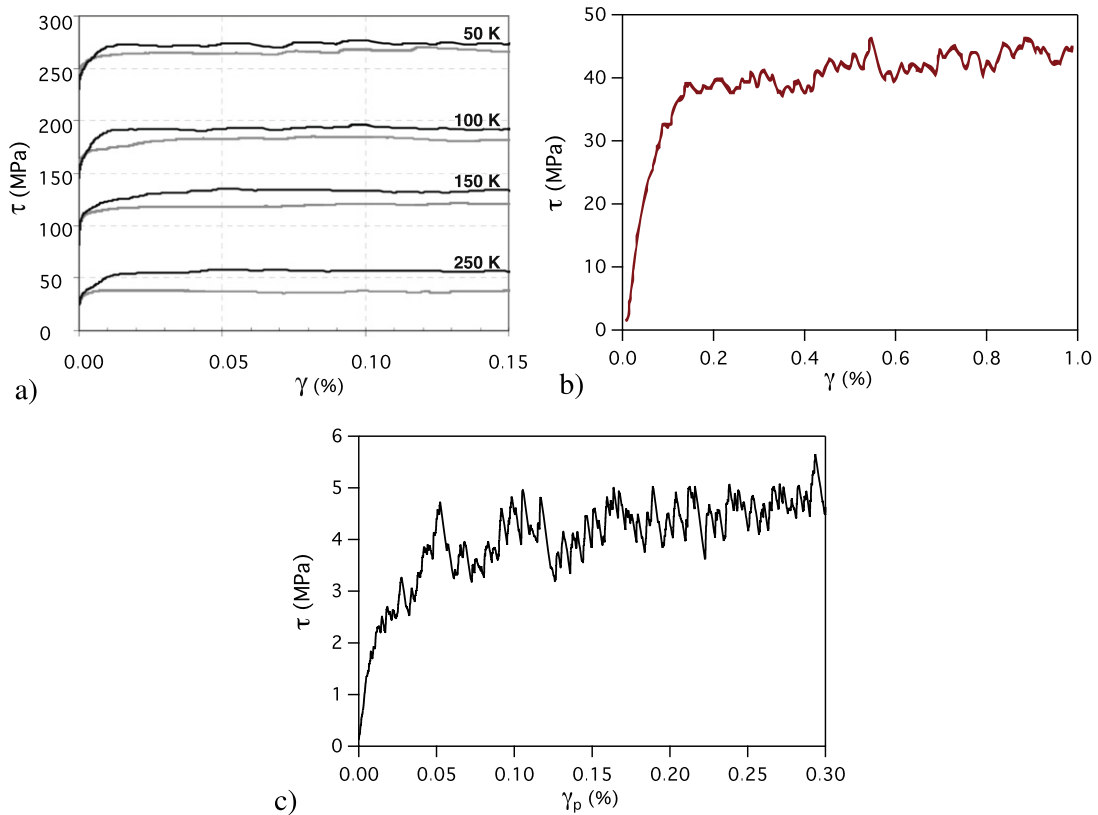
Fig. 1. Three examples of stress vs. strain curves yielded by 3D-DD simulations for different materials. a) Temperature dependence of the flow stress in α-iron single crystals in single slip, with (upper curves) and without (lower curves) a random distribution of carbides. All simulations were carried out at a constant strain rate of 10^{-4} s^{-1}. The mean particle size is 100 nm with a volume density of 3×10^{19} m^{-3} [9]. b) Tensile test in bcc ferrite with a random distribution of carbides in the athermal temperature regime ($T > 300$ K). Single slip conditions are imposed under a constant strain rate of 10 s^{-1}. The mean particle size is 100 nm with a volume density of 3×10^{19} m^{-3} [10]. c) [001] tensile test in a copper crystal deformed under a constant strain rate of 1 s^{-1}. Periodic boundary conditions were used in all calculations and the dimensions of the elementary cells are $5 \times 3 \times 3$ µm^3 (a), $2 \times 2 \times 2$ µm^3 (b), and $7 \times 10 \times 13$ µm^3 (c).

Fig. 1. Trois exemples de courbes contrainte – déformation obtenues par simulations de DD en 3D pour différents matériaux. a) Dépendance en température de la contrainte d'écoulement dans un monocristal de fer-α déformé en glissement simple, avec (courbes supérieures) et sans (courbes inférieures) une distribution aléatoire de carbures. Toutes les simulations ont été réalisées à une vitesse de déformation imposée de 10^{-4} s^{-1}. La taille moyenne des particules est de 100 nm avec une fraction volumique de 3×10^{19} m^{-3} [9]. b) Essai de traction dans une ferrite cc avec une distribution aléatoire de carbures et dans le régime athermique ($T > 300$ K). Des conditions de glissement simple sont imposées avec une vitesse de déformation constante de 10 s^{-1}. La taille moyenne des particules est de 100 nm avec une fraction volumique de 3×10^{19} m^{-3} [10]. c) Traction [001] sur un monocristal de Cu déformé à une vitesse de déformation imposée de 1 s^{-1}. Dans tous ces calculs, des conditions aux limites périodiques sont appliquées à des volumes simulés de dimensions $5 \times 3 \times 3$ µm^3 (a), $2 \times 2 \times 2$ µm^3 (b), et $7 \times 10 \times 13$ µm^3 (c).

of dislocation density with increasing strain is a function of the dislocation mobility. For lower, and more realistic values of B, plastic flow becomes jerky. This reflects the occurrence of an intermittent collective process (cf. Section 3). The strain dependencies of the flow stress and the dislocation density become independent of the free-flight velocity and plastic flow is controlled by the density of dislocation obstacles. In addition, an increase of the size of the simulated volume decreases the amplitude of the plastic bursts monitored on the stress vs. strain curves. This is because a given dislocation displacement is producing a smaller axial plastic strain increments with increasing specimen height. Indeed, macroscopic stress–strain curves are usually smooth, although intermittence is still present at a fine scale.

3. Dislocation avalanches in fcc metals

The mechanical response of materials where dislocation–dislocation interactions govern plastic flow presents large similarities. The most typical features are the occurrence of orientation-dependent deformation stages, which exhibit characteristic strain hardening behavior, and of patterned dislocation microstructures. There is as yet no well accepted model for dislocation patterning, whereas strain hardening is currently modeled in terms of average, uniform densities, as will be further discussed below.

The discrete nature of dislocation slip events is evidenced by the observation of slip traces at the surface of deformed crystals, which has been the object of many studies over the years. Slip events in fcc materials or simple hcp metals were
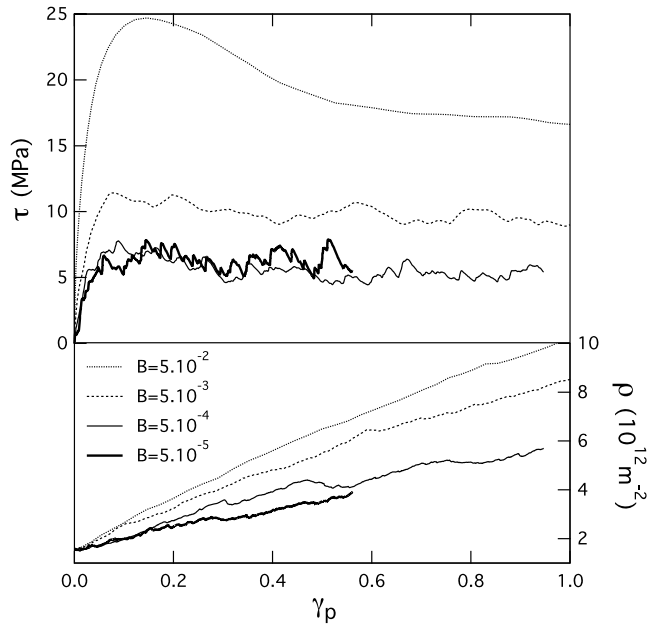
Fig. 2. Strain dependencies of the flow stress and dislocation density for increasing values of the viscous drag coefficient *B*. Tensile deformation of a copper crystal along a [001] loading axis under an imposed strain rate of 20 s^{-1}. The dimension of the elementary cell is $9.2 \times 10 \times 11.3$ μm^3 and periodic boundary conditions are used. The experimental value of *B* in copper at 300 K is approximately 5×10^{-5} Pa s^{-1}.

Fig. 2. Evolution de la contrainte d'écoulement et de la densité de dislocations en fonction de la déformation pour des valeurs croissantes du coefficient de frottement visqueux *B*. Traction d'un cristal de cuivre d'axe [001] à une vitesse de déformation imposée de 20 s^{-1}. Les dimensions du volume élémentaire simulé sont $9,2 \times 10 \times 11,3$ μm^3 avec des conditions aux limites périodiques. La valeur expérimentale de *B* dans le cuivre à 300 K est d'environ 5×10^{-5} Pa s^{-1}.

for instance described by Fisher et al. [12] as "avalanches separated in time". Cottrell [1] is also using the term "dislocation avalanches" to characterize these localized plastic strain bursts. The intermittent and scale-free nature of plastic flow in materials with low lattice friction was revealed in 2001 by acoustic emission studies in ice crystals [7]. This led to the development of statistical models (for a review, see [13]), which, as a rule, assume that dislocation avalanches are triggered by long-range interaction stresses between dislocations [14].

The strain bursts produced by avalanches are clearly visible in small crystals with dimensions in the micrometer range [8]. The same holds for DD simulations (cf. Fig. 1c), where the plastic strain bursts induce serrations in the stress vs. strain curves when the imposed loading is carried out in the equivalent of a stiff testing machine. A big dislocation avalanche occurring in a simulated copper crystal loaded along the [001] axis is shown in Fig. 3a. The burst of plastic flow is initiated by the unpinning of a single segment held by junctions with immobile forest obstacles. This segment expands rapidly under stress; it produces a transient mobile dislocation density and a small plastic strain increment. After having overcome a certain number of forest obstacles, the avalanche is eventually blocked at dislocation dense-regions, where it forms new junctions with attractive dislocation lines of the forest. During its operation, this avalanche produces the totality of the plastic strain recorded in the simulated sample.

The main outcome of these simulations is that dislocation avalanches are governed by junction processes. In parallel, a detailed examination of Fig. 3a shows that the forest segments are immobile during the strain burst. Therefore, short-range reactions are responsible for the occurrence of intermittent slip events and, in contrast to what is assumed in current models, long-range interactions do not play any significant role. Dislocation avalanches are critical phenomena because the triggering segment must overcome the resistance of localized obstacles, the junctions, before it expands in an irreversible manner. Another interesting feature that can be checked from Fig. 3a is that dislocation avalanches are blocked in regions where the density of forest obstacles is larger than average. This observation suggests making a connection between avalanches and the formation of dislocation patterns. Avalanches store dislocations in regions where the stored density already exhibits positive fluctuations. During plastic flow, the density of such regions evolves by an autocatalytic process: the denser they are, the larger is their probability of blocking avalanches, which further increases their density at a faster rate. After some plastic strain, the end product of such a process may be the formation of three-dimensional patterns of dislocation walls like the one shown in Fig. 4. Then, it may follow that pattern formation is not induced by long-range interaction stresses, as also postulated by current models [14].

It must be emphasized that dislocation avalanches are not necessarily planar because of the occurrence of cross-slip events. DD simulations confirm that dislocation cross-slip accelerates pattern formation [15], as was noted long ago by
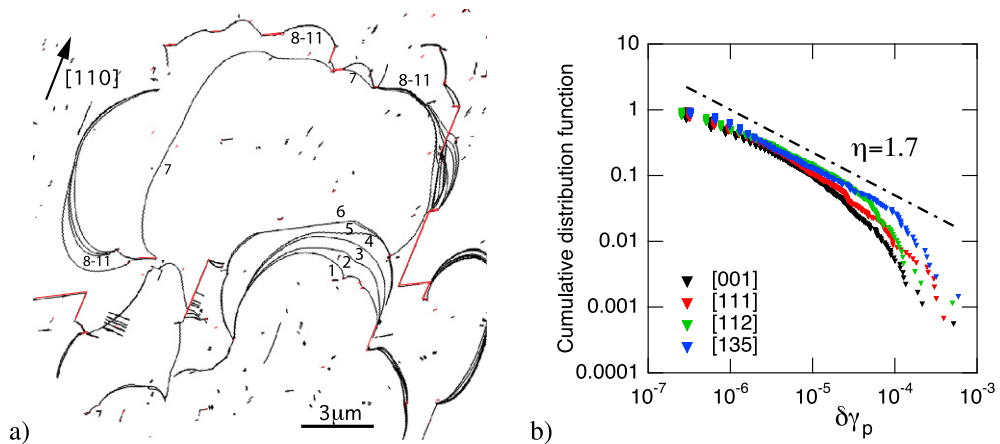
Fig. 3. a) Dislocation avalanche in a 3D-DD simulation of a tensile test in a [001] copper crystal at 300 K. The active Burgers vector during the avalanche is $b = \frac{1}{2}[110]$. It is seen in a thin foil of thickness 0.1 μm extracted along the $(\bar{1}11)$ active slip plane. The simulation was carried out with periodic boundary conditions. Short forest segments are seen cutting the glide plane of the mobile segments and junctions are highlighted in red. Eleven successive configurations taken at constant time intervals $\delta t = 0.4$ μs are superimposed. The avalanche is clearly triggered by the unzipping of a small junction at step 1. Between steps 5 and 6 the avalanche is slowed down by a dipolar interaction with a parallel dislocation lying outside the foil. The area swept before the avalanche is blocked by the formation of stable junctions at step 11 is about 160 μm². b) Cumulative distribution probabilities of strain burst amplitudes calculated from the simulated tensile deformation curves of copper crystals for four different orientations. The dotted line is a fit of the power-law given by Eq. (2), from which one deduces an exponent $\eta = 1.7$. The probability for observing large plastic avalanches is increasing with decreasing number of active slip systems, that is, when going from multislip orientations like [001] to the single slip orientation [135].

Fig. 3. a) Avalanche de dislocations lors de la simulation de DD en 3D d'un essai de traction [001] sur un cristal de cuivre à 300 K. Le vecteur de Burgers actif durant l'avalanche est $b = \frac{1}{2}[110]$. Les dislocations sont visualisées dans une lame mince d'épaisseur 0,1 μm et de normale $(\bar{1}11)$ contenant le plan de glissement actif. La simulation est réalisée avec des conditions aux limites périodiques. On voit de courts segments de forêt coupant le plan de glissement des dislocations mobiles et des jonctions tracées en rouge. Onze configurations prises à des intervalles de temps consécutifs de $\delta t = 0,4$ μs sont superposées. L'avalanche est clairement déclenchée à l'étape (1) par la destruction d'une courte jonction. Entre les étapes 5 et 6, l'avalanche est ralentie par interaction dipolaire avec un segment parallèle située en dehors de la lame. L'aire balayée par l'avalanche avant son arrêt à l'étape 11 est d'environ 160 μm². b) Distribution de probabilité cumulée des cisaillements plastiques dus aux avalanches sur des courbes contrainte – déformation simulées pour 4 orientations différentes dans le cuivre. La courbe en pointillés donne à partir de l'Eq. (2) un exposant $\eta = 1,7$. La probabilité d'observer de grandes avalanches augmente lorsque le nombre de systèmes de glissements actifs diminue, c'est à dire lorsque l'on passe d'une orientation de glissement multiple comme [001] vers une orientation de glissement simple comme [135].
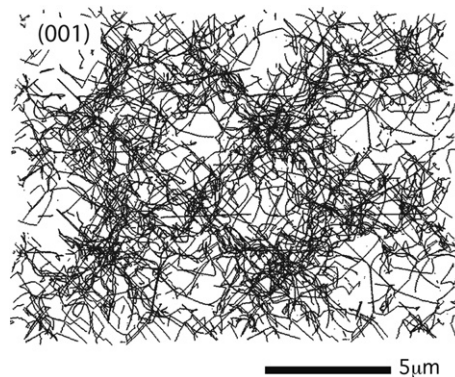

Fig. 4. Dislocation cell obtained under stress in a thin foil of thickness 5 μm extracted from a simulation of copper with periodic boundary conditions. The dimensions of the elementary cell are $5.8 \times 5.1 \times 4.6$ μm³ and the tensile axis is [001].

Fig. 4. Cellule de dislocations observée sous contrainte dans une lame mince d'épaisseur 5 μm extraite d'une simulation du cuivre avec des conditions aux limites périodiques. Les dimensions de la cellule élémentaire sont $5.8 \times 5.1 \times 4.6$ μm³ et l'axe de traction est [001].

Hirsch [16]. In addition, annihilations of screw and non-screw segments with forest dislocations lying in their cross-slip systems can also occur in an athermal manner [17].

The available results on the analysis of strain bursts show that the probability distribution function of their amplitude, $\delta\gamma$, take the general form of a power law [18]:

$$P(\delta\gamma) = C(\delta\gamma)^{-\eta} \exp\left[-(\delta\gamma/\delta\gamma_{\max})\right] \qquad (2)$$

where C is a normalization constant and η is a universal scaling exponent ($\eta = 1.5$–1.7). Fig. 3b shows that the results yielded by DD simulations are in the range of experimental values. The domain of scale-free behavior is probably bounded

at very low amplitudes because there is no stable configuration for non-reacting segments at too small approach distances of a junction. There is also a upper cut-off value for the amplitudes, $\delta\gamma_{\max}$ in Eq. (2), which is given by [18]:

$$\delta\gamma_{\max} = \frac{bE}{D(\theta + M)} \tag{3}$$

In this expression, E, θ and M are respectively the Young's modulus, a constant strain hardening coefficient and the combined stiffness of the specimen and testing apparatus. Λ is a characteristic specimen dimension. Eq. (3) expresses that the size of an avalanche is limited by stress relaxation in a stiff machine or by strain hardening under constant stress, so that the distance traveled by dislocations necessarily has an upper bound. The latter can be intrinsic to the dislocation structure in bulk single crystals, but it can also be limited by a free surface, a grain size, a spacing between twins, etc. The length D is, therefore microstructure-dependent and certainly contributes to the size effects observed in materials with small dimensions [8,18,19].

By comparing the distributions of avalanches for the various orientations shown in Fig. 3b, one can see that the maximum avalanche amplitudes decrease with increasing number of active slip systems, from the single slip orientation [135] to the [001] orientation that has the largest number of active slip systems. For these orientations, if the number of active slip systems is n, the number of forest systems is $(n - 1)$. Therefore, the maximum avalanche is experiencing a number of forest interactions per unit swept surface that increases with n. This property, which is probably common to the whole distribution of avalanches, goes in the same direction as the prediction of Eq. (3). However, it is not possible to define a strain hardening coefficient during the duration of an avalanche because the forest dislocations are immobile and their density remains constant.

One may note that since the avalanche distributions are bounded, it is justified to define an average avalanche of size $\bar{\Lambda}$, of which the amplitude shrinks with increasing number of active slip systems and increased forest density. This average avalanche also has another property. We consider the ratio of the perimeter of the avalanche, which is proportional to $\bar{\Lambda}$, to the swept area, which is proportional to $\bar{\Lambda}^2$. This ratio is proportional to $1/\bar{\Lambda}$. Thus, the smaller is the average size of dislocation avalanches, the larger is the storage rate of dislocations. The average size decreases when the forest, or total, density increases under stress or when the number of active slip systems increases from one orientation to the other. These specific properties of avalanches are the subject of an ongoing statistical study taking advantage of the data furnished by DD simulations. They can be retrieved in a formal manner, as will be shown in the next section.

We have noted that the notion of strain hardening rate, which is defined globally in a deforming specimen, has no meaning at the scale of an individual avalanche. It has, however, a meaning within the framework of current continuum models for crystal plasticity, where plastic flow is assumed to be smooth and uniform. The same holds for the density of mobile dislocations, which is defined only in a transient manner between the moment an avalanche begins and the moment it ends. At this last moment, the mobile density is transformed into a stored density. This raises the question of establishing a connection between the discrete plasticity events recorded at the mesoscale and dislocation-based continuum approaches of plastic flow and strain hardening.

4. Continuous dislocation-based modeling of crystal plasticity

Predicting on physical bases the mechanical response of crystalline materials is the ultimate goal of multiscale modeling. Because of the huge range in length and time scales involved from electronic structure computations to stress vs. strain curves of bulk samples, modeling steps are necessarily involved at some critical points. This is the case in particular for going from collective and discrete dislocation events at the mesoscale to continuum models that include dislocation-based constitutive formulations. This transition requires performing a coarse-graining procedure over representative volumes containing a statistically meaningful number of discrete events, which can be achieved with the help of DD simulations.

In the present case, the starting point for continuum modeling is provided by the well-known storage–recovery model, which was developed by Kocks [20] and Kocks and Mecking [21]. This model was further expanded by Teodosiu et al. [22] at the scale of dislocation slip systems. It is now widely used to describe the plastic deformation of polycrystals and is potentially well suited for the modeling of the complex orientation dependence of flow stress and strain hardening in single crystals of materials with low lattice resistance. Its main advantage is that it incorporates in dimensionless form the main elastic and core properties of dislocations. It yields, up to large strains and in a seamless manner, the evolution of all relevant variables like the dislocation densities and strains per slip system or the total strain hardening rate. Its drawbacks are that it contains a large number of unknown parameters and requires further modeling to incorporate collective dislocation behavior.

The connection to continuous and uniform plastic flow was performed with the help of DD simulations, of which the output also yields a response that can be decomposed per slip system. The parameters of the revisited storage–recovery model were drawn from the output of the simulations. As their values presented intermittent fluctuations, the latter were smoothened out, which yielded constant averaged values. This procedure, which is equivalent to an implicit coarse-graining, allowed performing a transition between discrete and continuous plastic flow in time and space. Like for the study of dislocation avalanches, periodic boundary conditions were used to obtain volume elements representative of the bulk material.

The storage–recovery model is based on two simplifying hypotheses. The first one is that there is always a sufficient mobile density to carry out the imposed strain rate, so that the evolution of this density during plastic flow does not need

Table 1

Values of the dimensionless parameters required to model strain hardening in fcc singe crystals. The first six columns give the interaction matrix coefficients (Eqs. (4)) measuring the strength of the interactions between slip systems [24]. The values were determined by modeling for the first two coefficients. For the four other ones, they were obtained by DD simulations and are given for a reference density of 10^{12} m^{-2}. The last three columns refer to the coefficients entering the definition of the mean free path for forest interactions in Eq. (5) [6]. Each value is an average of six to nine independent measurements, which yields error bars smaller than or equal to $\pm 5\%$ in most of the cases (see [6] for detail).

Tableau 1

Valeurs des paramètres sans dimension intervenant dans le modèle de durcissement plastique des monocristaux cfc. Les six premières colonnes correspondent aux coefficients de la matrice d'interaction entre systèmes de glissement (Eqs. (4)). Les deux premiers coefficients ont été déduits d'un modèle. Les quatre autres ont été calculées directement par des simulations de DD et sont données pour une densité de dislocations de référence de 10^{12} m^{-2}. Les trois colonnes suivantes donnent les coefficients intervenant dans le calcul du libre parcours moyen pour les interactions de la forêt (Eq. (5)). Toutes les valeurs données dans ce tableau sont issues de moyennes effectuées sur 6 ou 9 mesures indépendantes ce qui donne des barres d'erreur au plus égales à $\pm 5\%$ (voir [6] pour plus de détail).

a_0'	a_{copla}	a_{ortho}	a_2	a_3	a_{coli}	p_0	k_0	κ
0.122	0.122	0.07	0.137	0.127	0.625	0.117	1.08	0.29

to be modeled in detail. The mobile density is always small as compared to the density of stored dislocations, that is, of dislocations that are immobile at a given moment. As a consequence, the stored density can be assimilated to the total density. This assumption was justified a posteriori when the properties of dislocation avalanches were better understood. The mobile density only exists in a transient manner; it is produced by the expansion of a portion of dislocation loop and is stored by junction formation after having swept a certain area. Thus, the density stored at a given moment is the sum of all the previously stored transient mobile densities. Almost from the very beginning of plastic flow, it is practically identical to the total density. The second simplification is that the stored density is uniformly distributed in space. There is no clear justification for this assumption as yet, although it may be thought to follow from the scaling properties of the dislocation densities [23].

A first equation defines the critical stress τ_c^s for the activation of a slip system s as a function of the dislocation densities ρ^u stored in all slip systems u, including system s. This critical stress is derived from the following expression

$$\tau_c^s = \mu b \sqrt{\sum_u a^{su} \rho^u}; \quad \text{for the forest interactions } a_r^{su} = a_{ro}^{su} \left(\frac{\log 1/b\sqrt{a_{ro}^{su}\rho}}{\log 1/b\sqrt{a_{ro}^{su}\rho_o}} \right)^2 \tag{4}$$

where μ is the shear modulus. The first of Eqs. (4) looks similar to the traditional Taylor relation, but it is defined here in a different and broader context. In fcc crystals, the tensor a^{su} contains only six independent dimensionless coefficients, which account for the average strength of the six types of interactions occurring between slip systems. Four interactions lead to contact reactions between dislocations and are denoted a_r^{su}, where r stands for "reaction", in the second of Eqs. (4). Three of them lead to junction formation and the last one, the collinear interaction, leads to annihilations of dislocations with same Burgers vectors gliding in a slip system and its cross slip system. These interaction processes are essentially elastic in nature, but calculating their average strength at the scale of slip systems involves quite complex summations over a whole spectrum of local geometrical configurations. A specific type of DD simulations was devised to perform this averaging, in which mobile dislocations were let to interact with immobile forest densities leading to a specific type of reaction [24]. These simulations not only account for all types of reactions, they also include less strong contributions arising from the intersections of repulsive dislocations and from long range elastic interactions. It was found that the magnitude of the coefficients a_r^{su} decreases logarithmically with increasing dislocation density. This is expressed by the second of Eqs. (4), where ρ_o and a_{ro} represent reference values for a dislocation density of 10^{12} m^{-2}. This property results from the line energy of dislocations, which incorporates a logarithmic term with an outer cut-off radius scaling like $\rho^{-1/2}$. The logarithmic drift of interaction coefficients cannot be neglected when large variations of dislocation densities are considered, for instance upon modeling bulk materials up to large strains. The two remaining coefficients are associated with the interaction of a slip system with itself, or self-interaction, and the interaction between coplanar slip systems (coplanar interaction). In these cases, the determination of the interaction coefficients required some additional modeling. The values of the six interaction coefficients are given in Table 1. Estimating reasonably accurate values is critical for obtaining in a realistic manner the number and nature of the active slip systems, as well as the transitions at which new slip systems are activated under strain.

The strong point of the storage–recovery model is the description of the storage rate in terms of a geometrical length L, the *mean free path of dislocations*, which is defined from the storage rate of dislocations $d\rho/d\gamma$ by the relation $d\rho/d\gamma = 1/(bL)$. This scalar expression was first written by Kocks [20]. The mean free path of dislocations is understood in the continuum as the mean distance traveled by a mobile dislocation before it is stored. As a dislocation line expands while moving, L is somehow a virtual quantity that only makes sense during a small plastic strain increment such that the length of the mobile segment can be considered as almost constant. This is why the storage rate has to be expressed in differential form. It is intuitive that the mean free path of dislocations decreases with increasing stored density and depends on the strength of the dislocation obstacles opposing dislocation motion. A formal modeling of this quantity could be performed with the help of DD simulations [6,25]. The full expression of the storage rate is too complex to be reproduced here. Instead, we restrict ourselves to the rather simple form obtained for symmetrical loading conditions leading to the activation of two

or more slip systems. These slip systems then have same densities and critical stresses and they produce identical shear strains. For each slip system, and taking only into account the interactions between junction-forming forest slip systems, one has:

$$\left(\frac{\mathrm{d}\rho}{\mathrm{d}\gamma}\right)_f = \sum_{s\in f}\frac{\mathrm{d}\rho^s}{\mathrm{d}\gamma^s} = \frac{1}{L_f b} = \frac{\tau_c}{\mu b^2 K_{hkl}} \qquad (5)$$

where the index f indicates that only the storage rate induced by forest systems is considered, resulting in a mean free path L_f that is, as expected, inversely proportional to the critical stress τ_c. The dimensionless mean free path coefficient K_{hkl} is orientation-dependent. It is given by

$$K_{hkl} = \frac{n(1+\kappa)^{3/2}}{p_0\sqrt{a}k_0(n-1-\kappa)} \qquad (6)$$

In Eq. (6), n is the number of active slip systems, which influences the mechanical response in the same manner as for dislocation avalanches. With increasing values of n, the number of forest interactions increases as $(n-1)$, which results in an increased storage rate and, as will be seen below, an increased strain hardening rate. The three parameters, p_0, k_0 and κ that enter Eq. (6) are dimensionless constants for all fcc crystals [6]. They are defined as follows. Denoting by $\sqrt{a}$ the average interaction strength of junction-forming systems, the parameter p_0 is such that $p_0\sqrt{a}$ yields, within a geometrical constant, the probability for forming a stable junction upon crossing a forest obstacle. k_0 is related to the average length $\bar{\ell}$ of the dislocation segments pinned by junctions, which is inversely proportional to the critical stress: $\bar{\ell} = k_0\mu b/\tau_c$. The last parameter, κ, is the ratio of the junction density to the total density. It takes into account the contribution of the junction density to the total storage rate.

The full expression for the storage rate also includes simpler terms for the self-interaction [26] and the interaction between coplanar slip systems, which are not included in standard storage–recovery model [21]. These two terms required additional modeling [25]. The recovery part of the model accounts for dynamic recovery, that is, the thermally activated annihilations of screw dislocations by cross slip that induces a negative contribution to the total storage rate. This term is included in the original form of the storage–recovery model. It contains an unknown scaling length, the recovery length y, which is related to the cross-slip mechanism and the density of screw or nearly screw dislocations in the microstructure. The value $y^{123} = 0.5$ nm is adjusted to yield the experimental value of the critical stress τ_{III} for the onset of dynamic recovery for the [123] orientation. The orientation dependence of y^{hkl} can, nevertheless, be predicted by modeling from this single fitted value [27]. All these storage or recovery rates contribute in an additive manner to the net storage rate.

The equations of the storage–recovery model are set in closed form by adding a flow rule that accounts for the small strain rate sensitivity of fcc metals. The rather weak temperature and strain rate dependencies of the flow stress that manifest itself at low temperatures arise from jog formation upon repulsive intersections [2]. Therefore, the resolved applied stress τ_a^s on each slip system is written as the sum of the critical stress τ_c^s and of a small resolved thermal component. An expansion of the Arrhenius rate equation for jog formation at first order in $\tau_a^s - \tau_c^s$ yields an expression that is quite commonly used in continuum mechanics [28]:

$$\dot{\gamma}^s = \dot{\gamma}_0\left(\frac{\tau_a^s}{\tau_c^s}\right)^m \qquad (7)$$

where $\dot{\gamma}^s$ is the strain rate of system s, $\dot{\gamma}_0 = 10^{-3}$ s^{-1} is a reference strain rate and m is a constant related to the energetics of jog formation. For fcc metals, one typically has $m \approx 200$ around room temperature.

There are nine parameters of elastic origin in the equations of the fully developed storage–recovery model (Table 1), the six interaction coefficients entering Eqs. (4) and the three coefficients defining the mean free path constant K_{hkl} in Eq. (5). The measurement of these last three coefficients was performed by different methods on a number of simulations. It is important in two respects. First it confirmed that these parameters are really constants, irrespective of the fcc material considered. Second, it implies fitting continuous lines or curves to the fluctuating outputs of the DD simulations, thus establishing *de facto* a connection between intermittent dislocation behavior and continuous uniform flow (cf. Fig. 5).

A further check of the coefficient values listed in Table 1 can be performed by computing directly from DD simulations the values of the orientation-dependent coefficients K_{hkl} for symmetrical orientations and cross-checking the results with the prediction of Eq. (6), in which the values of p_0, k_0 and κ are inserted.

One can see from Eq. (5) that the positive storage rate of the forest is proportional to τ_c/K_{hkl}, hence to $\sqrt{a\rho}/K_{hkl}$ (Eqs. (4)). Thus, the stored density can be obtained by integrating the stored density with respect to strain, which yields a parabolic form containing the coefficients K_{hkl}. As illustrated by Fig. 5, these coefficients can then be determined directly from the strains and stored densities recorded at the output of DD simulations.

This figure clearly illustrates the orientation dependence of the mean free paths and of the stored densities. For instance, the slopes obtained for the [001] and [112] orientations differ by a factor of about two. In Table 2, the values of K_{hkl} are compared to the ones yielded by the model (Eq. (6)), using the coefficients given in Table 1. The agreement is excellent for the [111] and [112] orientations. For [001], the predicted value is further corrected to take into account an additional
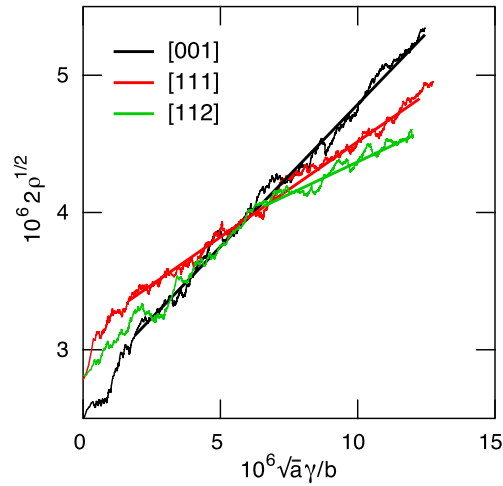
Fig. 5. Determination of the values of the mean free path coefficients by DD simulations for three symmetrical orientations. The slopes of the regression lines drawn through the intermittent output of the DD simulations yield the values of K_{hkl} given in Table 2, which are deduced from the total density ρ, the total plastic strain γ and the average strength of the active forest slip systems $\sqrt{a}$. These simulations were carried out at low stresses in order to avoid dynamic recovery. The measurements were performed after an initial transient during which a relevant stored density was accumulated.

Fig. 5. Mesure par DD des valeurs des trois coefficients intervenant dans le calcul du libre parcours moyen des dislocations pour trois orientations symétriques de l'axe de traction. Les pentes des courbes de régression ajustées sur les données des simulations donnent les valeurs de K_{hkl} reproduites dans la Table 2. Ces dernières se déduisent de la densité totale ρ, de la déformation et de la force d'interaction moyenne entre systèmes de glissement $\sqrt{a}$. Ces simulations ont été réalisées à faible contrainte pour éviter la restauration dynamique. Toutes les mesures sont effectuées au delà d'un transitoire pendant lequel se forme une microstructure réaliste.

Table 2

Cross-check of measurements of the mean free path constants for three symmetrical orientations. The line K_{mod} gives the value predicted by the model for the three mean free paths, using Eq. (6) and the coefficient values given in Table 1. The line K_{DD} gives values averaged over three sets of simulations. The last line $\theta_{II,mod}$ gives the values of the strain hardening coefficient in stage II, as predicted by the model [25].

Tableau 2

Vérification croisée de la mesure du libre parcours moyen pour trois orientations de glissement multiple en traction. La ligne K_{mod} donne les valeurs prédites par l'Eq. (6) du modèle prise avec les coefficients de la Table 1. La ligne K_{DD} donne les valeurs moyennes issues de trois simulations pour chaque coefficient. La dernière ligne donne les valeurs du coefficient d'écrouissage en stade II prédit par le modèle [25].

	[001]	[111]	[112]
K_{mod}	6.21	7.38	11.8
K_{DD}	5.0	7.3	10.1
$\theta_{II,mod.}$	$\approx \mu/150$	$\approx \mu/215$	$\approx \mu/300$

dislocation mechanism specific to this orientation that cannot be modeled [29]. The predicted strain hardening rates in stage II are then in perfect agreement with experiment [25].

Paradoxically, the expanded storage–recovery model allows understanding some properties of the dislocation avalanches. It is so because the mean free path, which is inversely proportional to stress and depends on orientation, is the continuous counterpart of the average size of avalanches, $\bar{\Lambda}$. It follows that the latter should depend on orientation, as was already noted in Section 3. More precisely, the mean free path decreases with increasing forest density, for instance through an increased number of active slip systems (cf. Eq. (6) and Table 2), and the average size of avalanches should exhibit the same orientation dependence. Furthermore, $\bar{\Lambda}$ was also found to decrease with increasing stress and should be inversely proportional to stress. If one further considers the possible relation between avalanche processes and pattern formation, the characteristic dimension of dislocation patterns should also be inversely proportional to stress. This is, indeed, a property of dislocation patterns that is experimentally well-known and has been extensively compiled (see for instance [30,31]).

Quite generally, what is usually called in plasticity the *similitude relation* between scaled characteristic dimensions and the inverse of scaled flow stresses does not hold only at low stresses, where the behavior is governed by elastic mechanisms. It is still valid in the dynamic recovery stage and well beyond. The origin of this scaling law can be traced back to the relation defining the average length of segments in the microstructure of deformed crystals, $\bar{\ell}$. As seen above, one has $\bar{\ell} = k_0 \mu b / \tau_c$, with $k_0 \approx 1.08$ (cf. Table 1). It follows from Eq. (4) that, for a given orientation, a similar and more fundamental relation exists between $\bar{\ell}$ and the densities stored in each slip system. For instance, in symmetrical conditions, one has $\bar{\ell} = k_0 / \sqrt{a\rho}$. As a consequence, dynamic recovery modifies the dislocation densities, which are stored at a smaller rate, but without modifying the similitude factor $k_0 / \sqrt{a}$ (within the logarithmic drift expressed by the second of Eqs. (4)).
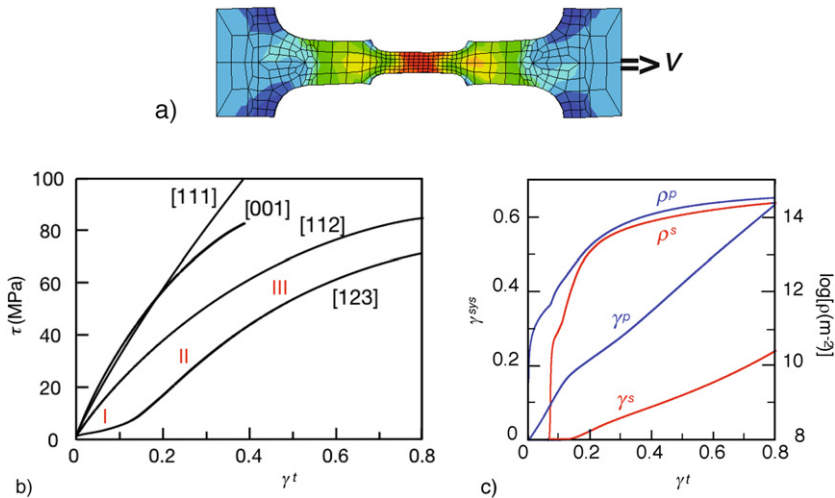
Fig. 6. Simulation of the mechanical response of copper single crystals using a crystal plasticity code and the dislocation-based storage–recovery model in its expanded form. The temperature is 300 K and the imposed strain rate is 10^{-4} s^{-1}. a) The meshed model specimen (under stress) used for the crystal plasticity simulations. The data are recorded in the central part of the gauge length, where the plastic strain is maximum and uniform. b) Resolved stress vs. total plastic strain curves for various orientations of the loading axis. Notice the strong orientation dependence of the deformation stages and the occurrence of the easy glide stage, or stage I, associated with single slip for the low-symmetry orientation [123]. c) The transition between stages I and II. The primary and secondary slip systems are denoted p and s. The evolution of their resolved shear strains γ and densities ρ are plotted as a function of the total resolved shear strain.

Fig. 6. Simulation de la réponse mécanique d'un monocristal de cuivre par un code de plasticité cristalline incluant le modèle généralisé pour l'évolution des densités de dislocations. La température est fixée à 300 K et la vitesse de déformation imposée est de 10^{-4} s^{-1}. a) Maillage de l'éprouvette simulée avec le code de plasticité cristalline (sous charge). Toutes les mesures sont réalisées dans la zone centrale de l'éprouvette où la déformation plastique est maximale et homogène. b) Courbe contrainte – déformation totale projetée pour différentes orientations de chargement. Noter la forte dépendance en orientation des stades de déformation et l'apparition d'un stade de glissement facile, le stade I, associé à l'orientations de faible symétrie [123]. c) Transition entre les stades I et II. Les systèmes primaire et secondaire sont notés p et s. L'évolution de leur déformation projetée γ et de leur densité ρ est tracée en fonction de la déformation totale projetée.

In the last step, the equations of the generalized model can be integrated to yield the mechanical response of fcc crystals as well as the strains and dislocation densities per slip system. The model parameters are the ones given in Table 1. Only one parameter has to be fitted to experiment, the dynamic recovery length for the [123] orientation. The integration is carried out in time and space for each slip system using a crystal plasticity code [32]. This type of code is a finite element code that is able to deal with slip geometry, in addition to the lattice rotations associated with dislocation glide. Boundary conditions for deformation in tension at a constant velocity are imposed to the meshed specimen shown in Fig. 6a.

Simulated tensile tests are shown in Fig. 6b for selected orientations with different symmetry and number of active slip systems. Without any *ad hoc* switch, the model reproduces in a realistic manner the traditional three-stage stress vs. strain curves and their characteristic strain hardening behavior. For the low-symmetry orientation [123], one obtains successively the single-slip stage I, with its characteristically low strain hardening rate, the linear and athermal stage II arising from forest interactions and, at a higher stress, the pseudo-parabolic stage III, during which dynamic recovery induces a decrease of the strain hardening rate. The strain hardening rates exhibit, as expected, significant orientation dependencies during stage II and the onset of stage III is also orientation-dependent. Fine detail like the cross-over between the stress vs. strain curves for the [111] and [001] orientations, which is experimentally observed, is well reproduced. It is explained by an interplay between the orientation dependencies of storage and dynamic recovery [27]. Fig. 6c illustrates another feature that is experimentally well-known. At the transition between stages I and II, a secondary slip system becomes active. Its density increases very fast and reaches the value of the primary density. Nevertheless, the primary density is responsible for most of the recorded plastic strain, because its mean free path is larger than that of the secondary system.

All these results are in excellent agreement with published experimental data (see for example [33]). One can notice the significant contrast between the rather large strains achieved at the scale of bulk specimens and the small strains used in the DD simulations for establishing the present constitutive formulation. It draws its origin to the use of dimensionless constants for all the mechanism that contribute to strain hardening.

5. Concluding remarks

This work illustrates the huge potential of mesoscale simulations for unraveling the physical aspects of crystal plasticity within a multiscale framework. Collective dislocation phenomena and strain hardening properties are long-standing problems, which can now be approached quantitatively and modeled in a predictive manner. In the present study on simple materials exhibiting no lattice resistance, scale transitions are performed between intermittent slip bursts at a fine

scale, a revisited version of the traditional storage–recovery model and the macroscopic response of fcc crystals. Dislocation dynamics simulations allowed successively to understand the role played by short-range interactions in the initiation and termination of dislocation avalanches, to perform a coarse-graining of intermittent behavior that yields an equivalent smooth and uniform behavior, to model a key quantity that governs strain hardening in continuum models, the mean free path of dislocations, to determine the values of the physical parameters involved in collective dislocation behavior and to establish a connection with continuum mechanics at the scale of slip systems, using crystal plasticity codes.

The development of these multiscale approaches is subject to several limitations. Their predictive ability is limited by the current knowledge on dislocation core properties, like cross slip in the present case, which is still insufficient to construct precise local rules for mesoscale simulations. Extensions to polycrystal plasticity or to complex deformation conditions seem feasible in the present stage, but cyclic deformation, during which plastic flow is partly reversible, requires additional modeling.

Finally, understanding size effects in materials with dimensions smaller than the typical size of dislocation avalanches presents a new challenge to multiscale modeling. Periodic boundary conditions can no longer be used and more complex boundary conditions including surface effects must be considered. In addition, the intrinsic heterogeneity of plastic flow becomes too strong to allow modeling in terms of continuous variables. Furthermore, DD simulations cannot make meaningful predictions as long as the mechanisms of dislocation multiplication or generation are poorly understood.

Acknowledgements

References

[1] A.H. Cottrell, Dislocations and Plastic Flow in Crystals, Clarendon Press, Oxford, 1953.
[2] J. Friedel, Dislocations, Pergamon Press, Oxford, 1967.
[3] J.P. Hirth, J. Lothe, Theory of Dislocations, Krieger, Malabar (Florida), 1992.
[4] V.V. Bulatov, L.P. Kubin, Curr. Opin. Solid State Mater. Sci. 3 (1998) 558–561.
[5] L. Kubin, G. Canova, M. Condat, B. Devincre, V. Pontikis, Y. Bréchet, Solid State Phenom. 23–24 (1992) 455–472.
[6] B. Devincre, T. Hoc, L. Kubin, Science 320 (2008) 1745–1748.
[7] M.-C. Miguel, A. Vespignagni, S. Zapperi, J. Weiss, J.-R. Grasso, Nature 410 (2001) 667.
[8] D. Dimiduk, C. Woodward, M. LeSar, M. Uchic, Science 312 (2006) 1188–1190.
[9] S. Naamane, Etude de la déformation plastique de la ferrite à basse température : Simulations de dynamique des dislocations, PhD thesis, Université Pierre et Marie Curie, 2008.
[10] S. Queyreau, Etude des mécanismes d'écrouissage sous irradiation de la ferrite par simulations de dynamique des dislocations, PhD thesis, Université Pierre et Marie Curie, 2008.
[11] D. Mordehai, Y. Ashkenazy, I. Kelson, G. Makov, Phys. Rev. B 74 (2006) 024112.
[12] J. Fisher, E. Hart, R. Pry, Phys. Rev. 87 (1952) 958–961.
[13] G. Ananthakrishna, Phys. Rep. 440 (2007) 113–239.
[14] M. Zaiser, A. Seeger, in: F.R.N. Nabarro, M.S. Duesbery (Eds.), Dislocations in Solids, vol. 11, Elsevier Science BV, Amsterdam, 2002, pp. 1–100.
[15] R. Madec, B. Devincre, L. Kubin, Scripta Mater. 47 (2002) 689–695.
[16] P. Hirsch, The Physics of Metals: 2. Defects, Cambridge University Press, Cambridge, UK, 1975.
[17] R. Madec, B. Devincre, L. Kubin, T. Hoc, D. Rodney, Science 301 (2003) 1879–1882.
[18] F. Csikor, C. Motz, D. Weygand, M. Zaiser, S. Zapperi, Science 318 (2007) 251–254.
[19] S. Lefebvre, B. Devincre, T. Hoc, J. Mech. Phys. Solids 55 (2007) 788–802.
[20] U. Kocks, J. Eng. Mater. Technol. 98 (1976) 76.
[21] U. Kocks, H. Mecking, Prog. Mater. Sci. 48 (2003) 171–273.
[22] C. Teodosiu, J.-L. Raphanel, L. Tabourot, in: C. Teodosiu, J.-L. Raphanel, F. Sidoroff (Eds.), Large Plastic Deformations, A.A. Balkema, Rotterdam, 1993, pp. 153–168.
[23] L. Kubin, B. Devincre, T. Hoc, Int. J. Mater. Res. 100 (2009) 1411–1419.
[24] B. Devincre, L. Kubin, T. Hoc, Scripta Mater. 54 (2006) 741–746.
[25] L. Kubin, B. Devincre, T. Hoc, Acta Mater. 56 (2008) 6040–6049.
[26] B. Devincre, L. Kubin, T. Hoc, Scripta Mater. 57 (2007) 905–908.
[27] L. Kubin, T. Hoc, B. Devincre, Acta Mater. 57 (2009) 2567–2575.
[28] E. Rauch, Etude de l'écrouissage des métaux : Aspects microstructuraux et Lois de comportement, Mémoire d'Habilitation, Ecole Nationale Supérieure de Physique de Grenoble, 1993.
[29] B. Devincre, L. Kubin, T. Hoc, Scripta Mater. 57 (2007) 905–908.
[30] M. Staker, D. Holt, Acta Metall. 20 (1972) 569–579.
[31] S. Raj, G. Pharr, Mater. Sci. Eng. A 81 (1986) 217–237.
[32] T. Hoc, C. Rey, J.L. Raphanel, Acta Mater. 49 (2001) 1835–1846.
[33] T. Takeuchi, Trans. JIM 16 (1975) 629–640.

---

[1] See "mM" home page at: http://zig.onera.fr/mm_home_page.